# Vibrational Relaxation of Highly Vibrationally Excited $O_3$ in Collisions with OH

**Lei Zhang,*,†,‡ Pingya Luo,† Zhiyu Huang,‡ Hong Chen,† and António J. C. Varandas*,§**

*State Key Laboratory of Oil and Gas Reservoir Geology and Exploitation, School of Chemistry and Chemical Engineering, Southwest Petroleum University, Chengdu 610500, Sichuan, People's Republic of China, and Departamento de Química, Universidade de Coimbra, 3004-535 Coimbra, Portugal*

*Received: April 28, 2008; Revised Manuscript Received: May 26, 2008*

We report a theoretical study of highly excited $O_3$ in collisions with vibrationally cold OH. Special emphasis is placed on initial vibrational energies of $O_3$ between 9 and 21 kcal mol$^{-1}$. All calculations have employed the quasiclassical trajectory method and the realistic double many-body expansion potential energy surface for $HO_4(^2A)$. Many aspects of the title relaxation process are presented. The results indicate that it may not be ignorable in studying the stratospheric ozone budget.

## 1. Introduction

Vibrationally excited molecules play a key role in a wide variety of areas in chemical dynamics and kinetics, and it is largely for this reason that the topic has been and remains a subject of much interest.[1–11] In particular, collisional relaxation of highly excited molecules is a primary mechanism by which hot molecular systems return to thermal equilibrium. A detailed knowledge of such processes is then key for accurately describing energy exchange processes responsible for thermal balance in atmospheric chemistry. In fact, to understand activated gas phase environments in which the populations of numerous species and states are often controlled by complex kinetic networks, one must know the extent to which vibrationally excited molecules resist collisional relaxation.[10,12] Not surprisingly, therefore, such processes have motivated much theoretical and experimental work.

The ozone molecule, both in its ground and vibrationally excited states, is of fundamental importance because it plays a crucial role in stratospheric and mesospheric chemistry. In fact, collisional processes involving atmospheric ozone have attracted much attention since Chapmans's pioneering studies in 1930. As the importance of ozone in controlling our planet's thermal and radiation budgets became evident, extensive efforts have been undertaken over the years to measure its properties, model its behavior in the atmosphere, and systematize an ever-increasing database of knowledge on this intriguing molecule.[8,9,13–20] Although significant progress has been made in understanding the reaction dynamics of the ozone molecule, complete characterization of the influence of vibrational excitation on the rates of such processes has remained elusive. Indeed, vibrationally excited $O_3$ [hereafter denoted by explicitly indicating its vibrational energy content: $O_3(E_v)$] is responsible for atmospheric infrared emission due to being a major contributor to the infrared luminosity of the upper atmosphere.[21,22] This provided a strong motivation for carrying out the present study of highly vibrationally excited $O_3$ colliding with OH, another key atmospheric species.

In a previous publication,[23] we have provided detailed information on the $O_3$ + OH atmospheric reaction with both reactants vibrationally excited. However, our understanding of the collisional energy transfer behavior of highly excited ozone molecules is far from complete since the role of vibrational relaxation in such processes has practically been ignored. Indeed, vibrational relaxation in collisional processes remains a significant source of uncertainty in the modeling of ozone infrared radiation and, hence, has important applications in the fields of atmospheric chemistry. In this respect, the ozone−hydroxyl bimolecular collisional process can be challenging for both theory and experiment. Thus, the need exists to obtain insights into its specific behavior and to identify important physical parameters and propensities in such a quenching process.

One of objectives of the study reported here is to provide detailed computations on the title vibrational relaxation process. Particular attention will be paid to $O_3(E_v)$ containing between 9 and 21 kcal mol$^{-1}$ of vibrational excitation, while the OH colliding partner molecules will be in their ground vibrational state. Thus, we cover the complete spectrum of possible excitations as the dissociation energy of hot ozone is ∼21 kcal mol$^{-1}$. Another is to test further our proposed double many-body expansion (DMBE) potential energy surface for ground-doublet $HO_4$,[24] which has been extensively used to study the important $OH(v) + O_3$ atmospheric reaction and its reverse,[24–27] and which has given results in good agreement with available experimental data. To achieve such goals, we will follow previous work by employing the well-established quasiclassical trajectory (QCT) method for the dynamics calculations. This is not only about the only viable means available for such a study but also is well-justified due to the high energy contents involved.

The paper is organized as follows. Section 2 provides a brief survey of the methodology. The results are presented and discussed in section 3, with concluding remarks in section 4.

## 2. Computational Details

Following previous work, we have employed the QCT method as implemented in the VENUS96[28] code, suitably adapted to study the title collisional processes. Calculations have been carried out for diatom−triatom translational energies over the range of $1.0 \leq E_{tr}$/kcal mol$^{-1}$ $\leq 12$, as summarized in Tables 1 and 2; some processes are not observed, being identified as

* Corresponding authors. E-mail: zgc166929@sohu.com (L.Z.), varandas@qtvs1.qui.uc.pt (A.J.C.V.).

† State Key Laboratory of Oil and Gas Reservoir Geology and Exploitation, Southwest Petroleum University.

‡ School of Chemistry and Chemical Engineering, Southwest Petroleum University.

§ Universidade de Coimbra.

10.1021/jp803686j CCC: $40.75 
Published on Web 07/12/2008

**TABLE 1: Summary of the Trajectory Calculations for OH + $O_3(E_v)$ Deactivation Processes[a]**

| | $E_{v_i} = 9$ kcal mol$^{-1}$ | | | $E_{v_i} = 15$ kcal mol$^{-1}$ | | $E_{v_i} = 21$ kcal mol$^{-1}$ | |
|---|---|---|---|---|---|---|---|
| $\Delta E_\downarrow$ | $E_{tr}$ | $b_{max}$ | $\sigma^{\Delta E_\downarrow} \pm \Delta\sigma^{\Delta E_\uparrow}$ | $b_{max}$ | $\sigma^{\Delta E_\downarrow} \pm \Delta\sigma^{\Delta E_\uparrow}$ | $b_{max}$ | $\sigma^{\Delta E_\downarrow} \pm \Delta\sigma^{\Delta E_\uparrow}$ |
| −1 | 1.0 | 10.77 | 145.25 ± 3.99 | 11.15 | 132.00 ± 4.13 | 11.72 | 108.89 ± 4.19 |
| | 2.0 | 10.02 | 118.65 ± 3.14 | 10.39 | 114.71 ± 3.59 | 10.96 | 98.69 ± 3.71 |
| | 4.0 | 9.26 | 93.07 ± 2.86 | 9.64 | 88.85 ± 3.00 | 10.20 | 78.19 ± 3.12 |
| | 6.0 | 8.50 | 77.47 ± 2.41 | 8.88 | 72.49 ± 2.52 | 9.45 | 66.61 ± 2.67 |
| | 8.0 | 7.75 | 64.12 ± 2.00 | 8.13 | 61.82 ± 2.12 | 8.69 | 61.72 ± 2.33 |
| | 12.0 | 8.13 | 55.07 ± 2.05 | 8.50 | 52.59 ± 2.14 | 8.88 | 53.28 ± 2.28 |
| −2 | 1.0 | 10.77 | 41.92 ± 2.60 | 11.15 | 60.73 ± 3.16 | 11.72 | 52.61 ± 3.16 |
| | 2.0 | 10.02 | 39.39 ± 2.33 | 10.39 | 52.77 ± 2.75 | 10.96 | 47.74 ± 2.81 |
| | 4.0 | 9.26 | 35.42 ± 2.04 | 9.64 | 41.00 ± 2.27 | 10.20 | 42.53 ± 2.46 |
| | 6.0 | 8.50 | 32.37 ± 1.78 | 8.88 | 34.70 ± 1.92 | 9.45 | 38.85 ± 2.17 |
| | 8.0 | 7.75 | 30.08 ± 1.54 | 8.13 | 30.19 ± 1.64 | 8.69 | 33.23 ± 1.84 |
| | 12.0 | 8.13 | 26.66 ± 1.55 | 8.50 | 26.13 ± 1.62 | 8.88 | 28.50 ± 1.77 |
| −3 | 1.0 | 10.77 | 8.75 ± 1.25 | 11.15 | 16.79 ± 1.77 | 11.72 | 25.88 ± 2.29 |
| | 2.0 | 10.02 | 7.41 ± 1.07 | 10.39 | 14.76 ± 1.55 | 10.96 | 23.77 ± 2.05 |
| | 4.0 | 9.26 | 6.46 ± 0.92 | 9.64 | 12.55 ± 1.32 | 10.20 | 22.41 ± 1.85 |
| | 6.0 | 8.50 | 5.34 ± 0.77 | 8.88 | 12.02 ± 1.19 | 9.45 | 19.07 ± 1.58 |
| | 8.0 | 7.75 | 4.71 ± 0.66 | 8.13 | 11.10 ± 1.04 | 8.69 | 16.62 ± 1.35 |
| | 12.0 | 8.13 | 3.83 ± 0.63 | 8.50 | 10.22 ± 1.05 | 8.88 | 13.26 ± 1.24 |
| −4 | 1.0 | 10.77 | nr[b] | 11.15 | 8.20 ± 1.25 | 11.72 | 18.76 ± 1.97 |
| | 2.0 | 10.02 | nr | 10.39 | 6.28 ± 1.02 | 10.96 | 15.47 ± 1.67 |
| | 4.0 | 9.26 | nr | 9.64 | 4.67 ± 0.82 | 10.20 | 11.61 ± 1.35 |
| | 6.0 | 8.50 | nr | 8.88 | 3.72 ± 0.67 | 9.45 | 10.24 ± 1.18 |
| | 8.0 | 7.75 | nr | 8.13 | 3.32 ± 0.58 | 8.69 | 8.90 ± 1.01 |
| | 12.0 | 8.13 | nr | 8.50 | 2.27 ± 0.51 | 8.88 | 8.30 ± 1.00 |
| −6 | 1.0 | 10.77 | nr | 11.15 | 1.76 ± 0.58 | 11.72 | 8.84 ± 1.37 |
| | 2.0 | 10.02 | nr | 10.39 | 1.19 ± 0.45 | 10.96 | 7.74 ± 1.20 |
| | 4.0 | 9.26 | nr | 9.64 | 0.73 ± 0.33 | 10.20 | 6.71 ± 1.04 |
| | 6.0 | 8.50 | nr | 8.88 | 0.74 ± 0.30 | 9.45 | 4.77 ± 0.81 |
| | 8.0 | 7.75 | nr | 8.13 | 0.72 ± 0.27 | 8.69 | 3.44 ± 0.63 |
| | 12.0 | 8.13 | nr | 8.50 | 0.70 ± 0.26 | 8.88 | 2.97 ± 0.60 |

[a] Units are with the energies in kcal mol$^{-1}$, impact parameters in $a_0$, and cross section in $a_0^2$. [b] Not relevant.

**TABLE 2: Summary of the Trajectory Calculations for OH + $O_3(E_v)$ Activation Processes[a]**

| | $E_{v_i} = 9$ kcal mol$^{-1}$ | | | $E_{v_i} = 15$ kcal mol$^{-1}$ | | $E_{v_i} = 21$ kcal mol$^{-1}$ | |
|---|---|---|---|---|---|---|---|
| $\Delta E_\uparrow$ | $E_{tr}$ | $b_{max}$ | $\sigma^{\Delta E_\uparrow} \pm \Delta\sigma^{\Delta E_\uparrow}$ | $b_{max}$ | $\sigma^{\Delta E_\uparrow} \pm \Delta\sigma^{\Delta E_\uparrow}$ | $b_{max}$ | $\sigma^{\Delta E_\uparrow} \pm \Delta\sigma^{\Delta E_\uparrow}$ |
| 1 | 1.0 | 10.77 | 6.92 ± 1.11 | 11.15 | 4.88 ± 0.97 | 11.72 | 2.80 ± 0.77 |
| | 2.0 | 10.02 | 12.61 ± 1.38 | 10.39 | 10.18 ± 1.29 | 10.96 | 3.77 ± 0.84 |
| | 4.0 | 9.26 | 16.57 ± 1.45 | 9.64 | 14.59 ± 1.42 | 10.20 | 7.80 ± 0.82 |
| | 6.0 | 8.50 | 19.31 ± 1.42 | 8.88 | 17.35 ± 1.41 | 9.45 | 11.22 ± 1.22 |
| | 8.0 | 7.75 | 20.75 ± 1.32 | 8.13 | 18.67 ± 1.33 | 8.69 | 14.24 ± 1.26 |
| | 12.0 | 8.13 | 22.61 ± 1.44 | 8.50 | 20.45 ± 1.45 | 8.88 | 16.11 ± 1.37 |
| 2 | 1.0 | 10.77 | nr[b] | 11.15 | nr | 11.72 | 0.22 ± 0.22 |
| | 2.0 | 10.02 | 0.16 ± 0.16 | 10.39 | 0.33 ± 0.24 | 10.96 | 1.32 ± 0.50 |
| | 4.0 | 9.26 | 1.08 ± 0.38 | 9.64 | 1.75 ± 0.50 | 10.20 | 3.27 ± 0.73 |
| | 6.0 | 8.50 | 1.93 ± 0.47 | 8.88 | 3.35 ± 0.64 | 9.45 | 5.75 ± 0.89 |
| | 8.0 | 7.75 | 3.77 ± 0.59 | 8.13 | 4.25 ± 0.66 | 8.69 | 8.43 ± 0.98 |
| | 12.0 | 8.13 | 8.82 ± 0.94 | 8.50 | 5.11 ± 0.75 | 8.88 | 8.92 ± 1.03 |
| 3 | 1.0 | 10.77 | nr | 11.15 | nr | 11.72 | nr |
| | 2.0 | 10.02 | nr | 10.39 | nr | 10.96 | 0.19 ± 0.19 |
| | 4.0 | 9.26 | nr | 9.64 | nr | 10.20 | 0.32 ± 0.32 |
| | 6.0 | 8.50 | nr | 8.88 | nr | 9.45 | 1.40 ± 0.44 |
| | 8.0 | 7.75 | nr | 8.13 | nr | 8.69 | 2.84 ± 0.58 |
| | 12.0 | 8.13 | nr | 8.50 | nr | 8.88 | 3.10 ± 0.62 |

[a] Units are with the energies in kcal mol$^{-1}$, impact parameters in $a_0$, and cross section in $a_0^2$. [b] Not relevant.

"not relevant". In all cases the initial rotational quantum number of the colliding OH has been fixed at its ground level ($j = 1$). Although a more rigorous kinetics treatment would involve an average over all initial rotational states, such a mammoth task is probably unjustified on the basis of previous work.[26,27] Thus, we omit heretofore the specification of the initial rotational state. In turn, $E_v = \sum_{k=1}^{3} E_{v_k}$ will denote the total vibrational energy of $O_3$, with $E_{v_k}$ indicating the energy content of the various vibrational normal modes of the triatomic molecule. Note that the chosen vibrational excitation energy range for $O_3(E_v)$ covers internal energies of the triatomic up to near dissociation. Note further that, as in previous work of this series, the rotational energy about each principal axis of inertia of $O_3$ has been taken as $k_B T/2$, whereas the rotational temperature has been assumed to be 300 K. This corresponds to an intermediate value in the range of temperatures $100 \leq T/\mathrm{K} \leq 500$, which covers the range of interest in atmospheric chemistry. The initial diatom−triatom separation has been fixed at $17a_0$ to make the interaction essentially negligible, and the optimum step size for integration of the equations of motion has been set according to the usual

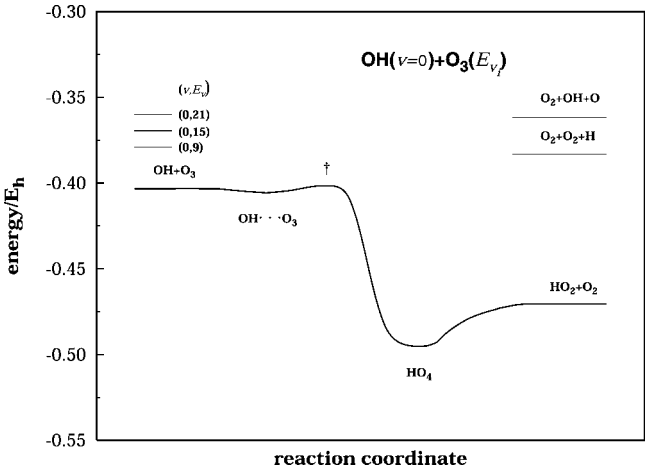


**Figure 1.** Schematic diagram showing the energetics of different processes according to the $HO_4$ DMBE potential energy surface.

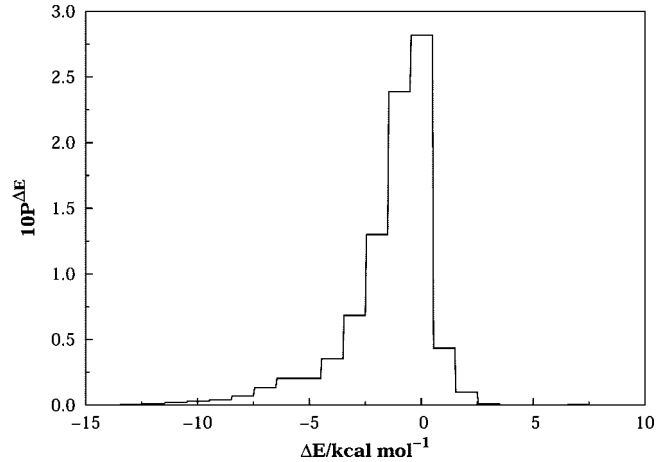


**Figure 2.** Vibrational state-to-state energy-transfer probability distributions.

procedure. In turn, the maximum value of the impact parameter ($b_{max}$) leading to vibrational relaxation has been optimized from batches of 200 trajectories. This ensured that the standard deviation between the vibrational energy of the products in the nonreactive trajectories and the vibrational energy of the reactants has a similar value as for the total energy conservation (this is typically of 0.01 kcal $mol^{-1}$). Batches of 2000 trajectories have then been carried out at each translational energy and initial vibrational combination, making a total (for all combinations) of $3.6 \times 10^4$ trajectories.

The energetics of the involved processes are best seen from the diagram of Figure 1, where we have indicated by the line segments on the reactants side the various vibrational combinations according to the $HO_4$ DMBE potential energy surface.[24] Note that all internal energy combinations of the reactants are not only quite above the energy of the transition state for reaction leading to $HO_2(v) + O_2$ but also higher than the energy of the products channel leading to $O_2 + O_2 + H$ formation. Although such reactive collisions will then be feasible over the complete range of translational energies, we will focus on the nonreactive events.

The procedure for describing the state-to-state energy transfer arising from the title relaxation process is best explained in terms of a scheme which involves the following steps. For a specific initial vibrational excitation of ozone, $O_3(E_{v_i})$, we count the trajectory outcomes according to their vibrational energy content and set $\Delta E$ (in kcal $mol^{-1}$) at the amount of transferred vibrational energy. A negative value of $\Delta E$ indicates the loss of energy by $O_3(E_{v_i})$ in a deactivation process, whereas a positive one refers to energy gain via an activation mechanism. Thus, we have defined the state-bin as encompassing the range of $(E_{v_i} + \Delta E) - 0.5 \rightarrow (E_{v_i} + \Delta E) + 0.5$ and considered as vibrationally inelastic trajectories for losing/gaining $\Delta E$ kcal $mol^{-1}$ all those whose vibrational energy falls inside such a bin. Needless to say, the above boxing scheme suffers from the usual errors inherent to the partition of the internal energy.[28] This problem has been tentatively overcome by leaving an interval of 1 kcal $mol^{-1}$ around the starting energy to account for such errors.

For a given value of the translational energy, the deactivation cross section is given by $\sigma^{\Delta E_i} = \pi b_{max}{}^2 P^{\Delta E_i}$, with the associated 68% uncertainties given by $\Delta\sigma^{\Delta E_i} = [(N - N^{\Delta E_i})/(NN^{\Delta E_i})]^{1/2}\sigma^{\Delta E_i}$; thus, $N^{\Delta E_i}$ is the number of trajectories that lead upon de-excitation to an energy transfer of up to $\Delta E$ out of a total of $N$ collisions starting with an initial vibrational energy of $E_{v_i}$, and $P^{\Delta E_i} = N^{\Delta E_i}/N$ is the corresponding vibrational de-excitation probability. From the deactivation cross section and assuming a Maxwell−Boltzmann distribution over the translational energy, the state-to-state thermal rate coefficients are obtained as

$$k^{\Delta E_i}(T) = g_e(T)\left(\frac{2}{k_B T}\right)^{3/2}\left(\frac{1}{\pi\mu}\right)^{1/2}\int_0^\infty E_{tr}\sigma^{\Delta E_i}\exp\left(-\frac{E_{tr}}{k_B T}\right)dE_{tr} \quad (1)$$

where $g_e(T) = [1 + \exp(-205/T)]^{-1}$ is the electronic degeneracy factor which corresponds to the ratio of the electronic partition functions, $k_B$ is the Boltzmann constant, $\mu$ is the reduced mass of the colliding particles, and $T$ is the temperature. Analogous expressions are defined for the activation process.

## 3. Results and Discussion

Tables 1 and 2 provide a summary of the trajectory calculations. Note that the maximum impact parameter shows a tendency to increase with internal energy of the reactants for a fixed translational energy. Conversely, $b_{max}$ tends to increase with decreasing translational energy. These observations may be rationalized by the fact that the de-excitation process involves the coupling of the various degrees of freedom, possibly induced by long-range (electrostatic dipole−dipole and dipole−quadrupole) interactions. It should be recalled that although the DMBE formalism (ref 29 and references therein) has been intended to include explicitly the long-range (electrostatic, induction, and dispersion) interactions into the potential energy surface, this has only been done for $HO_4$ up to the four-body electrostatic (and this only for the $HO_3$ fragment) and three-body dispersion terms. Thus, one should expect only an approximate description of the interaction between the permanent electric dipole and quadrupole moments of the OH and $O_3$ fragments.

Figure 2 displays the vibrational state-to-state energy-transfer probability distributions for $O_3(E_v)$ with initial vibrational energies of 21 kcal $mol^{-1}$. For simplicity, only the case corresponding to $E_{tr} = 4.0$ kcal $mol^{-1}$ is shown in Figure 2. Both deactivation and activation processes involving frequently multiquantum transitions are observed. Such a mechanism may be justified on the basis of reasonably strong (mostly of the electrostatic type) long-range interactions and invoking that an extensive energy change between the vibrational modes is required. Another interesting feature from this figure is perhaps the fact that the collisional deactivation process originates $\Delta E$ values up to −12 kcal $mol^{-1}$, supporting the existence of

**TABLE 3: Energies (in kcal mol$^{-1}$) Partitioned to Different Degrees of Freedom in the OH + $O_3$($E_{v_i}$ = 21) Deactivation Processes**

| | | | $O_3$ | | OH | |
|---|---|---|---|---|---|---|
| $\Delta E_{\downarrow}$ | $E_{tr}$ | $\langle E_{tr}\rangle$ | $\langle E_v\rangle$ | $\langle E_r\rangle$ | $\langle E_v\rangle$ | $\langle E_r\rangle$ |
| −1 | 1.0 | 0.92 | 20.00 | 1.62 | 5.23 | 0.27 |
| | 2.0 | 1.72 | 20.01 | 1.55 | 5.25 | 0.39 |
| | 4.0 | 3.23 | 20.01 | 1.65 | 5.26 | 0.52 |
| | 6.0 | 4.77 | 20.00 | 1.74 | 5.25 | 0.73 |
| | 8.0 | 6.25 | 19.98 | 1.91 | 5.26 | 0.95 |
| | 12.0 | 9.54 | 20.01 | 2.01 | 5.29 | 0.98 |
| −2 | 1.0 | 1.31 | 19.09 | 1.81 | 5.20 | 0.69 |
| | 2.0 | 1.97 | 19.08 | 1.92 | 5.19 | 0.84 |
| | 4.0 | 3.46 | 19.08 | 2.11 | 5.25 | 0.84 |
| | 6.0 | 5.16 | 19.05 | 2.08 | 5.25 | 1.03 |
| | 8.0 | 6.79 | 19.06 | 2.10 | 5.25 | 1.25 |
| | 12.0 | 9.98 | 19.07 | 2.34 | 5.24 | 1.26 |
| −3 | 1.0 | 1.72 | 18.05 | 1.97 | 5.12 | 1.27 |
| | 2.0 | 2.43 | 18.06 | 2.03 | 5.20 | 1.31 |
| | 4.0 | 3.98 | 18.05 | 2.05 | 5.09 | 1.71 |
| | 6.0 | 5.13 | 18.08 | 2.77 | 5.21 | 1.59 |
| | 8.0 | 6.72 | 18.07 | 2.73 | 5.25 | 1.81 |
| | 12.0 | 10.34 | 18.06 | 2.91 | 5.16 | 1.77 |
| −4 | 1.0 | 1.91 | 17.06 | 2.14 | 5.12 | 1.90 |
| | 2.0 | 2.61 | 17.05 | 1.81 | 5.25 | 2.30 |
| | 4.0 | 3.96 | 16.99 | 2.58 | 5.18 | 2.19 |
| | 6.0 | 5.67 | 17.11 | 2.43 | 5.35 | 2.18 |
| | 8.0 | 7.75 | 17.02 | 2.26 | 5.25 | 2.35 |
| | 12.0 | 10.25 | 17.07 | 3.39 | 5.32 | 2.32 |
| −6 | 1.0 | 3.42 | 14.95 | 1.87 | 5.03 | 2.84 |
| | 2.0 | 3.01 | 15.05 | 2.41 | 5.21 | 3.35 |
| | 4.0 | 4.85 | 15.06 | 2.53 | 5.73 | 3.39 |
| | 6.0 | 6.67 | 14.95 | 2.95 | 5.32 | 2.94 |
| | 8.0 | 8.95 | 15.03 | 2.26 | 5.45 | 2.88 |
| | 12.0 | 11.59 | 15.05 | 4.01 | 5.05 | 2.69 |

collisions that transfer large amounts of energy. The exponential energy-gap law, a propensity in agreement with other vibrational relaxation processes,[10,30,31] is therefore introduced to adequately describe the long tail of the energy-transfer probability distribution. Since similar considerations apply to other initial vibrational excitations of $O_3$, we further suggest that, for a fixed translational energy, the shape of the energy-transfer distribution will not significantly vary with the initial vibrational energy, with the amplitude of the multiquantum transitions in the deactivation process increasing with the internal energy content of the donor species. Thus, one expects more states to be populated upon deactivation.

Table 3 provides a summary of the information on the products energy partitioning for the deactivation process of $O_3(E_v)$ with $E_{v_i}$ = 21 kcal mol$^{-1}$. Three remarks are in order. First, the average value of the vibrational energy in the acceptor OH molecule is never found to exceed that of the first vibrationally excited level. This implies that a considerable part of the transferred internal energy has been channeled into rotational and translational degrees of freedom. Thus, one expects a small probability for vibration−vibration (V−V) energy transfer to occur (in this case the hot molecule would lose vibrational energy for the acceptor species which would become vibrationally excited). As a result, a vibration to rotation/translation (V−R, V−T) energy-transfer mechanism seems to be responsible for the bulk of the deactivation processes here reported. Of course, in classical mechanics one cannot exclude that some vibrational energy will flow into rotation prior to close contact of the two interacting species, although contact may be considered to occur whenever the electronic densities of the two molecules start to overlap each other. Second, for $\Delta E \geq -2$ kcal mol$^{-1}$, the (average) final translational energies are never found to exceed the corresponding initial translational energies, which implies that the V−T energy transfer should be small. Thus, one may conclude that the V−R mechanism is dominant in the deactivation process. In fact, compared with the initial rotational energy of ozone, the (average) final rotational energies increase by about 0.7−1.2 kcal mol$^{-1}$. However, for $\Delta E < -2$ kcal mol$^{-1}$, the ratios between the (average) final and initial translational energies tend to decrease with initial translational energy. This suggests that the dependence of energy transfer on the relative translational energy shows two different patterns. For low translational energies, the deactivation process is the result of V−T and V−R energy transfers, whereas for high translational energies the V−R mechanism seems to offer the best route for deactivation. Third, the percent rotational energy of the final $O_3$ molecule increases with translational energy. Thus, the rotational degrees of freedom of the energy-donor triatomic play a significant role in the collisional deactivation process. The results further suggest that deactivation based on V−R energy exchange occurs primarily via collisions that simply redistribute the energy in the hot $O_3$ molecule, converting vibrational to rotational energy. Similar considerations apply to the corresponding activation processes, as shown in Table 4. Note that, for the studied relative translational energy regimes, most of the energy transferred in such processes is via a T → V mechanism.

**TABLE 4: Energies (in kcal mol$^{-1}$) Partitioned to Different Degrees of Freedom in the OH + $O_3$($E_{v_i}$ = 21) Activation Processes**

| | | | $O_3$ | | OH | |
|---|---|---|---|---|---|---|
| $\Delta E_{\uparrow}$ | $E_{tr}$ | $\langle E_{tr}\rangle$ | $\langle E_v\rangle$ | $\langle E_r\rangle$ | $\langle E_v\rangle$ | $\langle E_r\rangle$ |
| 1 | 1.0 | 0.80 | 21.82 | 0.50 | 4.63 | 0.41 |
| | 2.0 | 0.99 | 21.87 | 0.74 | 5.25 | 0.25 |
| | 4.0 | 2.33 | 21.86 | 1.03 | 5.13 | 0.59 |
| | 6.0 | 3.71 | 21.90 | 1.23 | 5.21 | 0.63 |
| | 8.0 | 5.26 | 21.88 | 1.42 | 5.23 | 0.75 |
| | 12.0 | 8.52 | 21.89 | 1.51 | 5.25 | 0.99 |
| 2 | 1.0 | 0.60 | 22.68 | 0.92 | 2.79 | 1.14 |
| | 2.0 | 0.87 | 22.84 | 1.24 | 3.84 | 0.36 |
| | 4.0 | 1.66 | 22.86 | 1.10 | 4.86 | 0.53 |
| | 6.0 | 2.73 | 22.85 | 1.44 | 5.14 | 0.74 |
| | 8.0 | 4.20 | 22.94 | 1.45 | 5.19 | 1.01 |
| | 12.0 | 7.42 | 22.93 | 1.77 | 5.23 | 1.18 |
| 3 | 1.0 | 0.51 | 24.20 | 0.74 | 2.42 | 0.24 |
| | 2.0 | 0.67 | 24.42 | 0.84 | 3.14 | 0.62 |
| | 4.0 | 1.20 | 23.81 | 0.90 | 3.97 | 1.26 |
| | 6.0 | 2.30 | 23.82 | 1.30 | 4.98 | 0.66 |
| | 8.0 | 3.90 | 23.88 | 1.32 | 4.93 | 0.88 |
| | 12.0 | 6.67 | 23.91 | 1.44 | 5.36 | 1.34 |

We now examine the shape of the specific state-to-state cross sections versus translational energy which is shown in Figure 3 for $E_{v_i}$ = 21 kcal mol$^{-1}$. In this figure, panel a corresponds to the deactivation process, and panel b corresponds to the activation one. Although not shown, similar patterns are observed for other cases. Clearly, two opposite trends are visible which explain the observed shapes. The deactivation cross sections show a strong decrease with translational energy, suggesting that a capture-like mechanism (arising from the strong coupling of the available degrees of freedom governed by the long-range interactions) operates over the whole range of translational energies. Thus, one observes a behavior similar to the one operating in the reactive case.[27] Conversely, for the activation process, the common pattern found in reactions that have an energy threshold is observed: the activation cross section increases with translational energy until it eventually reaches a maximum (as one may conjecture from the observed plateau)

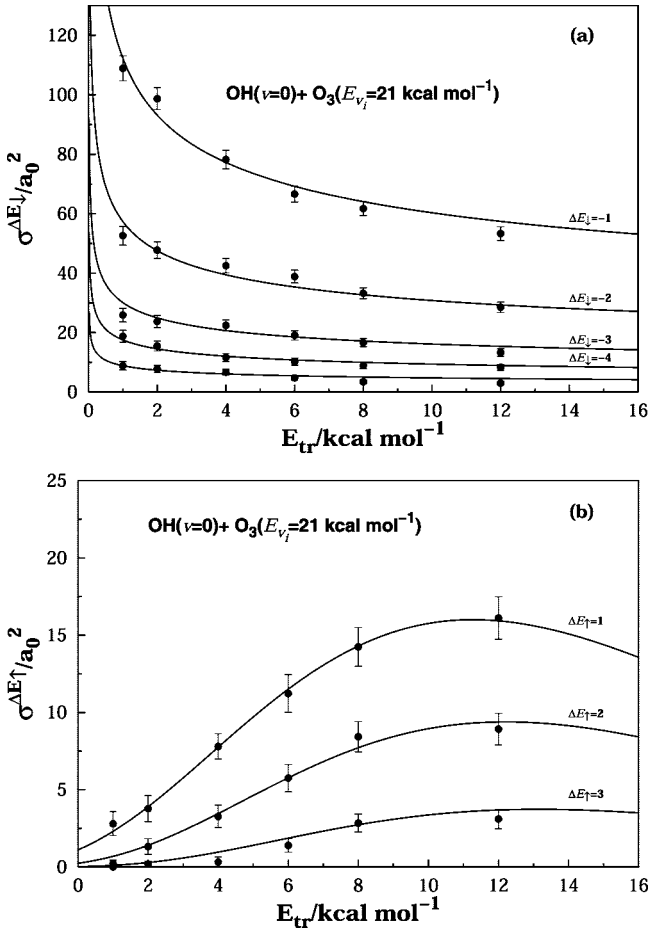


**Figure 3.** Cross sections as a function of the translational energy for $E_{v_i}$ = 21 kcal mol$^{-1}$: (a) $\sigma^{\Delta E_\downarrow}$; (b) $\sigma^{\Delta E_\uparrow}$. Also indicated are the 68% error bars and the fitted line given by eqs 2 and 3.

and decreases afterwords. The dependence of the deactivation cross section on translational energy may be described by the form

$$\sigma^{\Delta E_\downarrow}(E_{OH}, E_{O_3}, E_{tr}) = \frac{\sum_{i=1}^{7} c_i E_{sum}^i}{E_{tr}^{n_1}} \quad (2)$$

whereas the activation part has been modeled by

$$\sigma^{\Delta E_\uparrow}(E_{OH}, E_{O_3}, E_{tr}) = \left(\sum_{j=0}^{2} d_j E_{sum}^j\right)[E_{tr} - E_{tr}^{th}]^{n_2} \exp[-m(E_{tr} - E_{tr}^{th})] \quad (3)$$

where

$$E_{tr}^{th} = a + bE_{sum} \quad (4)$$

and $E_{sum} = E_{OH} + E_{O_3}$, with $E_{OH}$ and $E_{O_3}$ being the internal energies of OH and $O_3$ molecules. Thus, the above representation depends on the internal energy of the reactants but not on any specific model that expresses the dependence of the internal energy on the quantum numbers. The optimum parameters obtained by least-squares are reported in Table 5, whereas the fitted functions are shown jointly with the calculated points in Figure 3. Clearly, the fit reflects the general trends of the calculations, although one cannot claim that such a representation is unique or even reflects unambiguously the underlying physics of the process.

**TABLE 5: Numerical Values of Least-Squares Parameters in eqs 2 and 3**[a]

| parameter | $E_{v_i} = 9$ | $E_{v_i} = 15$ | $E_{v_i} = 21$ |
|---|---|---|---|
| $c_1$ | 1.2253(2)[b] | −7.0116(2) | 1.3807(2) |
| $c_2$ | 2.0971(2) | 3.1681(2) | −5.3638(−1) |
| $c_3$ | −1.0843(2) | −5.8174(1) | 8.5509 |
| $c_4$ | 2.0083(1) | 5.5563 | −0.7160 |
| $c_5$ | −1.8007 | −0.2910 | 3.3211(−2) |
| $c_6$ | 7.9163(−2) | 7.9155(−2) | 8.0942(−4) |
| $c_7$ | −1.3686(−3) | −8.7178(−5) | 8.1061(6) |
| $n_1$ | 0.3513 | 0.3481 | 0.2702 |
| $n_2$ | 1.5029 | 0.8559 | 3.8346 |
| $d_0$ | 0.9281 | 1.3216 | 0.9282 |
| $d_1$ | 1.2552 | 4.6163 | −5.2879(−2) |
| $d_2$ | −7.2474(−2) | −0.1986(−6) | 7.4008(−4) |
| $m$ | 0.1177 | 7.1880(−2) | 0.2616 |
| $a$ | −1.1014(2) | −3.1099(1) | −2.9828(1) |
| $b$ | 6.6502 | 1.3931 | 0.9359 |

[a] Units are with the energy in kcal mol$^{-1}$, the cross section in $a_0^2$. [b] Given in the parentheses are the powers of 10 by which the numbers should be multiplied.

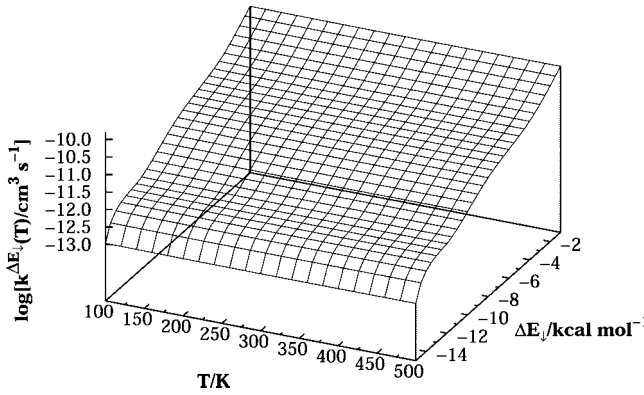


**Figure 4.** Thermal deactivation rate coefficient for OH + $O_3$($E_{v_i}$ = 21 kcal mol$^{-1}$) as a function of temperature.

By substitution of eqs 2–4 in eq 1 and performing the integration analytically, one obtains for the specific state-to-state deactivation and activation rate coefficients

$$k^{\Delta E_\downarrow}(T) = g_e(T)\left(\frac{8}{\pi\mu}\right)^{1/2}\left(\sum_{i=1}^{7} c_i E_{sum}^i\right)\Gamma(2 - n_1)(RT)^{-n_1+1/2} \quad (5)$$

and

$$k^{\Delta E_\uparrow}(T) = g_e(T)\left(\frac{8}{\pi\mu}\right)^{1/2}\left(\left(\sum_{j=0}^{2} d_j E_{sum}^j\right)\frac{(RT)^{n_2+1/2}\exp[-E_{tr}^{th}/RT]}{(1 + mRT)^{n_2+2}} \times \left[\Gamma(n_2 + 2) + \Gamma(n_2 + 1)(1 + mRT)E_{tr}^{th}/RT\right]\right) \quad (6)$$

where $\Gamma(...)$ is the gamma function, and all other symbols have their usual meaning. Figure 4 shows as a perspective plot of the OH + $O_3$($E_{v_i}$ = 21) deactivation rate constant as a function of temperature and de-excitation energy $\Delta E_\downarrow$. Similar trends are observed for other values of $E_{v_i}$ studied in the present work. Since their shapes differ only quantitatively, we show only the first case in Figure 4. The notable feature is perhaps the decrease of the rate constant with decreasing de-excitation $\Delta E_\downarrow$.

## 4. Conclusions

We have reported a theoretical study of the title relaxation processes which, to our knowledge, provides the first information of energy transfer in collisions of vibrationally excited $O_3$ with ground-state OH. The calculations predict the relaxation of hot ozone to occur primarily via V−R and V−T mechanisms. Specifically, V−R is found to dominate in the deactivation process at high translational energy regimes, whereas the V−V exchange energy process generally plays a minor role. The calculations further suggest that the deactivation process is to a large extent governed by the long-range interactions as shown by the capture-like shape of the calculated excitation function. Conversely, the activation process shows the usual form of excitation function. As for practical implications, it is concluded that vibrational relaxation may not be ignorable when discussing the ozone budget in the middle atmosphere. No comparison with experimental data has been possible due to unavailability of the latter. Clearly, experimental efforts toward the study of the title processes would be welcome.

**Acknowledgment.** Financial support from Sichuan Provincial Science and Technology Fund for Distinguished Young Scholars (07ZQ026-016) with the SRF for ROCS(SEM[2007]1108,MOP [2006]164) and NKBRP(2005CB221300) is gratefully acknowledged. The financial support to one of us (A.J.C.V.) from Fundação para a Ciência e Tecnologia, Portugal (Contracts POCI/QUI/60501/2004, POCI/AMB/60261/2004, and REEQ/128/QUI/2005), under the auspices of POCI 2010 of Quadro Comunitário de Apoio III cofinanced by FEDER, is also gratefully acknowledged.

## References and Notes

(1) Muller, U.; Stock, G. *J. Chem. Phys.* **1997**, *107*, 6230.
(2) Weston, R. E.; Flynn, G. W. *Annu. Rev. Phys. Chem.* **1992**, *43*, 559.
(3) Gilbert, R. G.; Smith, S. C. *Theory of Unimolecular and Recombination Reactions*; Blackwell Scientific Publications: Oxford, 1990.
(4) Oref, I.; Tardy, D. C. *Chem. Rev.* **1990**, *90*, 1407.
(5) Gordon, R. *Comments At. Mol. Phys.* **1988**.
(6) Miller, R. L.; Suits, A. G.; Houston, P. L.; Toumi, R.; Mack, J. A.; Wodtke, A. M. *Science* **1994**, *265*, 1831–1838.
(7) Rogaski, C. A.; Price, J. M.; Mack, J. A.; Wodtke, A. M. *Geophys. Res. Lett.* **1993**, *20*, 2885.
(8) Varandas, A. J. C. *Int. Rev. Phys. Chem.* **2000**, *19*, 199.
(9) Varandas, A. J. C. *ChemPhysChem* **2002**, *3*, 433.
(10) Varandas, A. J. C. *J. Phys. Chem. A* **2004**, *108*, 758.
(11) Varandas, A. J. C. *J. Phys. Chem. A* **2005**, *109*, 2700.
(12) Bevilacqua, T. J.; Weisman, R. B. *J. Chem. Phys.* **1993**, *98*, 6316.
(13) Baulch, D. L.; Cox, R. A. *J. Phys. Chem. Ref. Data* **1980**, *9*, 295.
(14) Baulch, D. L.; Cox, R. A.; Crutzen, P. J.; Kerr, J. A.; Troe, J.; Watson, R. T. *J. Phys. Chem. Ref. Data* **1982**, *11*, 327.
(15) *Global Ozone Research and Monitoring Project*; Watson, R. T. Ed., 1985.
(16) Steinfeld, J. I.; Adler-Golden, S. M.; Gallagher, J. W. *J. Phys. Chem. Ref. Data* **1987**, *16*, 911.
(17) Eluszkiewicz, M. A. J.; Allen, M. *J. Geophys. Res.* **1993**, *98*, 1069.
(18) Osterman, G. B.; Salawitch, R. J.; Sen, B.; Toon, G. C.; Stachnik, R. A.; Pickett, H. M.; Margitan, J. J.; Blavier, J.; Peterson, D. B. *Geophys. Res. Lett.* **1997**, *24*, 1107.
(19) Crutzen, P. *Science* **1997**, *277*, 1951.
(20) Caridade, P. J. S. B.; Zhang, L.; Garrido, J. D.; Varandas, A. J. C. *J. Phys. Chem. A* **2001**, *105*, 4395.
(21) Stair, A. T.; Baker, D. J.; Wyatt, C. L.; Baker, K. D. *Geophys. Res. Lett.* **1974**, *1*, 117.
(22) Stair, A. T.; Ulwick, J. C., Jr.; Baker, D. J.; Baker, K. D. *Atmospheres of the Earth and the Planets*; McCormack, B. M. Ed.; D. Reidel Publishing Company: Dordrecht, The Netherlands, 1975; p 335.
(23) Zhang, L.; Luo, P. Y.; Huang, Z. Y.; Varandas, A. J. C. *J. Phys. Chem. A* **2006**, *110*, 13836.
(24) Varandas, A. J. C.; Zhang, L. *Chem. Phys. Lett.* **2000**, *331*, 474.
(25) Zhang, L.; Varandas, A. J. C. *Phys. Chem. Chem. Phys.* **2001**, *3*, 1439.
(26) Zhang, L.; Varandas, A. J. C. *J. Phys. Chem. A* **2001**, *105*, 10347.
(27) Zhang, L.; Varandas, A. J. C. *J. Phys. Chem. A* **2002**, *106*, 11911.
(28) Hase, W. L.; Duchovic, R. J.; Hu, X.; Komornicki, A.; Lim, K. F.; Lu, D.; Peslherbe, G. H.; Swamy, K. N.; Linde, S. R. V.; Varandas, A. J. C.; Wang, H.; Wolf, R. J. *QCPE Bull.* **1996**, *16*, 43.
(29) Varandas, A. J. C. In *Conical Intersections: Electronic Structure, Spectroscopy and Dynamics*; Domcke, W., Yarkony, D. R., Köppel, H. Eds.; Advanced Series in Physical Chemistry; World Scientific Publishing, 2004; Chapter 5, p 91.
(30) Forst, W.; Penner, A. P. *J. Chem. Phys.* **1980**, *72*, 1435.
(31) Bollati, R. A.; Ferrero, J. C. *J. Phys. Chem.* **1994**, *98*, 3933.

JP803686J